

Dissecting chromatin interactions in living cells from protein mobility maps

Fabian Erdel · Katharina Müller-Ott ·
Michael Baum · Malte Wachsmuth ·
Karsten Rippe

Published online: 17 September 2010
© Springer Science+Business Media B.V. 2010

Abstract The genome of eukaryotes is organized into a dynamic nucleoprotein complex referred to as chromatin, which can adopt different functional states. Both the DNA and the protein component of chromatin are subject to various post-translational modifications that define the cell's gene expression program. Their readout and establishment occurs in a spatio-temporally coordinated manner that is controlled by numerous chromatin-interacting proteins. Binding to chromatin in living cells can be measured by a spatially resolved analysis of protein mobility using fluorescence microscopy based approaches. Recent advancements in the acquisition of protein mobility data using fluorescence bleaching and correlation methods provide data sets on diffusion coefficients, binding kinetics, and cellular concentrations on different time and length scales. The combination of different techniques is needed to dissect the

complex interplay of diffusive translocations, binding events, and mobility constraints of the chromatin environment. While bleaching techniques have their strength in the characterization of particles that are immobile on the second/minute time scale, a correlation analysis is advantageous to characterize transient binding events with millisecond residence time. The application and synergy effects of the different approaches to obtain protein mobility and interaction maps in the nucleus are illustrated for the analysis of heterochromatin protein 1.

Keywords Fluorescence microscopy · Fluorescence correlation spectroscopy · Fluorescence recovery after photobleaching · Heterochromatin protein 1

Abbreviations

ACF	Autocorrelation function
CD	Chromodomain
CLSM	Confocal laser scanning microscopy
CP	Continuous fluorescence photobleaching
dfFCS/2fFCS	Dual-focus FCS
EMCCD	Electron-multiplying charge-coupled device
GFP (RFP, CFP, YFP)	Green (red, cyan, yellow) fluorescent protein
FRAP	Fluorescence recovery after photobleaching

Fabian Erdel and Katharina Müller-Ott shared first author.

F. Erdel · K. Müller-Ott · M. Baum · K. Rippe (✉)
Deutsches Krebsforschungszentrum and BioQuant,
Research Group Genome Organization and Function,
Im Neuenheimer Feld 280,
69120 Heidelberg, Germany
e-mail: Karsten.Rippe@dkfz.de

M. Wachsmuth
European Molecular Biology Laboratory,
Cell Biology and Biophysics Unit,
Meyerhofstr. 1,
69117 Heidelberg, Germany

FCS	Fluorescence correlation spectroscopy
FCCS	Fluorescence cross-correlation spectroscopy
FLIP	Fluorescence loss in photobleaching
FRET	Fluorescence resonance energy transfer
HP1	Heterochromatin protein 1
ICS	Image correlation spectroscopy
LSFM	Light sheet-based fluorescence microscopy
mfFCS	Multifocal FCS
MSD	Mean squared displacement
pCP	Point CP
pFCS	Point FCS
pFRAP	Point FRAP
ROI	Region of interest
RICS	Raster image correlation spectroscopy
SCF	Spatial autocorrelation function
SDCM-FCS	Spinning disk confocal microscopy-FCS
sFCS	Scanning FCS
STICS	Spatio-temporal image correlation spectroscopy
STFM	Spatial and temporal fluctuation microscopy
TICS	Temporal image correlation spectroscopy
TIRF	Total internal reflection fluorescence

Introduction

The eukaryotic genome is organized by histone proteins into a highly dynamic and polymorphic complex termed chromatin (van Holde 1989). Large local variations of the chromatin composition exist with respect to the presence and absence of so-called epigenetic modifications of DNA and histones (methylation, acetylation, phosphorylation, etc.) and of associated protein complexes as inferred from genome-wide mapping studies (Campos and Reinberg 2009; Lee and Mahadevan 2009). Different functional chromatin states are established by regulatory epigenetic networks that control the accessibility of the

DNA for transcription, DNA repair and replication machineries. The underlying networks operate via the highly dynamic chromatin binding of proteins that recognize specific epigenetic modifications of histones and DNA, set or remove these, recruit epigenetic modifiers to certain sites or serve as architectural chromatin components (Campos and Reinberg 2009; McBryant et al. 2006; Taverna et al. 2007).

Fluorescence microscopy-based methods are ideally suited to measure chromatin interactions in single living cells. Spatially resolved protein mobility data are related to images of cellular structures from fluorescence confocal laser scanning microscopy (CLSM) to identify localization-specific dynamics and interactions of a fluorescently labeled species (Wachsmuth et al. 2008). The spatial resolution of the mobility and interaction analysis is usually restricted by the diffraction-limited size of the excitation volume in a confocal fluorescence microscopy setup with typical dimensions of at least $200 \times 200 \times 600$ nm. The fluorescent tagging is conducted frequently via fusion of the protein of interest with a green/cyan/yellow/red autofluorescent domain (GFP, CFP, YFP, RFP) (Wang et al. 2008). The fluorescent labeling of epigenetic modifications in living cells is less well established and a currently emerging field (Kimura et al. 2010). Approaches include for example (1) the detection of DNA methylation via binding of a 5-methyl-cytosine-binding domain fused to GFP and a nuclear localization signal (Yamagata et al. 2007), (2) a chromatin-incorporated histone H4 construct that shows a fluorescence resonance energy transfer signal between CFP and a YFP variant that depends on the acetylation state of lysines 5 and 8 (Sasaki et al. 2009), and (3) the microinjection of an antibody fragment that recognizes the H3S10 phosphorylation (Hayashi-Takanaka et al. 2009).

To measure protein mobility three groups of approaches can be distinguished: One group relies on local photo-induced bleaching (or activation) of fluorescence and a subsequent evaluation of the spatial distribution of the fluorescence signal over time. This approach is used by FRAP (fluorescence recovery after photobleaching) (Axelrod et al. 1976; Peters et al. 1974), continuous fluorescence photobleaching (CP) or fluorescence loss in photobleaching (FLIP) (Cole et al. 1996; Cutts et al. 1995; Peters et al. 1981; Wachsmuth et al. 2003). The second group of approaches uses the

intensity signal fluctuations of fluorescent molecules entering and leaving the focal volume of a confocal microscope. In fluorescence correlation spectroscopy (FCS) these fluctuations are evaluated by a so-called temporal autocorrelation analysis as reviewed previously (Haustein and Schwille 2007; Wachsmuth et al. 2008; Wachsmuth and Weisshart 2007). The third group of approaches measures the translocation of individual particles directly over time (Li and Elf 2009; Siebrasse et al. 2007). Such single particle tracking methods represent a direct approach to identify diffusive translocations and binding events of a molecule of interest. However, they are frequently limited to relatively short observation periods (<1 s) over which the fluorescence signal can be detected and a rather small number of trajectories that can be acquired for the analysis. Here, we focus on the acquisition of protein mobility maps obtained by the currently available repertoire of bleaching and correlation methods that provide a spatial resolution at or near the diffraction limit, i.e., the focal volume of a confocal microscope (Fig. 1). Theoretical considerations for analyzing protein mobility data are summarized. Finally, the application of fluorescence microscopy based methods to the analysis of chromatin interactions of heterochromatin protein 1 (HP1) is discussed.

Measuring spatially resolved dynamics and interactions

Bleaching and correlation measurements at a single point

Point fluorescence recovery after photobleaching

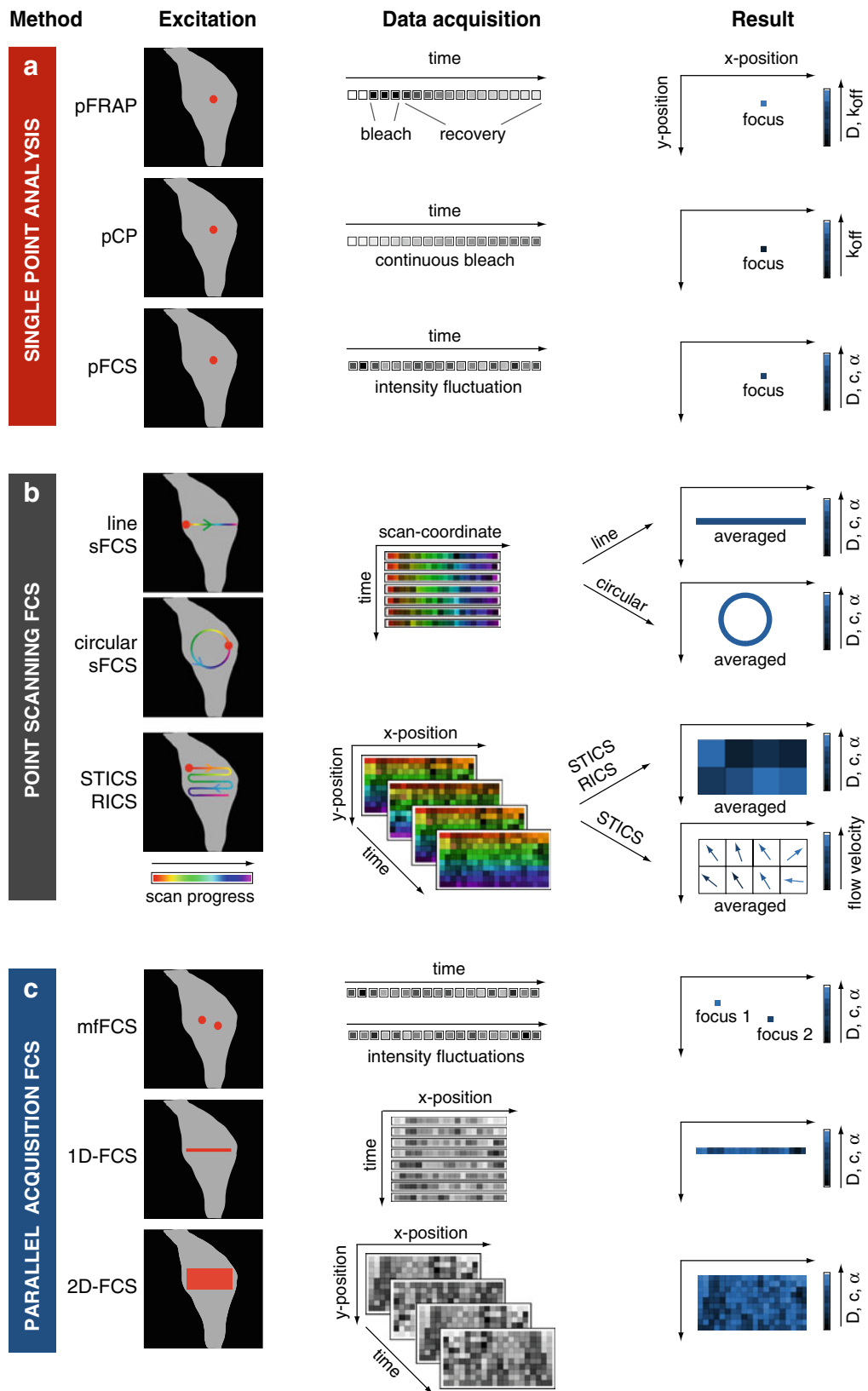
Fluorescence recovery after photobleaching is a widely used photobleaching technique to investigate protein mobilities within living cells. FRAP monitors the redistribution of fluorescently labeled molecules back to an equilibrium state resulting from diffusion or directed transport into a cellular region of interest after having bleached most fluorophores in this region with high intensity laser illumination (Fig. 1a). Imaging-based FRAP measurements are limited by the efficiency of the bleaching process (multiple bleaching steps may be required for highly photostable fluorophores) as well as the acquisition speed of the fluorescence recovery for the microscope used. The latter usually requires at least a few tens of

milliseconds to acquire one image, i.e. diffusion coefficients below $1\text{--}10\text{ }\mu\text{m}^2\text{ s}^{-1}$ can be measured. The drawback of the slow acquisition speed can be overcome by point FRAP (pFRAP), which uses the small observation volume of a confocal microscope fixed at a position of interest to record pre- as well as post-bleach intensities within this focal volume (Table 1). Taking advantage of this very small bleaching and observation volume (submicrometer dimensions) and a sensitive detection system, shorter bleaching periods and much lower pre- and post-bleach intensities are possible. Furthermore, single-point detection allows a much higher temporal resolution below the millisecond range (Table 1) (Schmidt et al. 2009; Wachsmuth et al. 2008).

Point continuous fluorescence photobleaching

In point CP, the focus of a confocal system is fixed at a desired position in a cell and the decrease of fluorescence in the so-defined observation volume is recorded under continuous illumination (Fig. 1a) (Peters et al. 1981). Gradually, a dynamic equilibrium between association to and dissociation from immobile structures, diffusion/transport, and photobleaching is established. This is represented by a characteristic decay of the fluorescence signal which often shows biphasic behavior: a fast initial decay mainly from bleaching of an immobilized or slowly mobile/transiently bound fraction fades into a slow asymptotic decay originating from bleaching of the whole pool of freely mobile molecules exchanging with the bound fraction. Thus, from inspection of the shape of the CP curve one can distinguish the case of fully diffusive or fully immobilized molecules or a mixture of slowly diffusive and transiently bound molecules. Since the bleaching and observation volume of a point CP experiment are sufficiently well-defined a quantitative analysis can also be conducted (Delon et al. 2006; Wachsmuth et al. 2003). It yields the different fractions and properties of the binding reaction. Moreover, the focus volume dimensions are small in relation to the diffusion distances on the relevant time scale so that the conditions for a pseudo-first order approximation of the immobilization reaction are met in most cases when the bleaching and the dissociation rate are of the same order of magnitude.

Single-point fluorescence correlation spectroscopy FCS employs thermal concentration fluctuations in an equi-



◀ **Fig. 1** Fluorescence microscopy-based methods for the investigation of protein mobility in living cells with high spatial resolution. Methods are classified according to the geometry of the excitation setup. For references see Table 1. **a** Single-point measurements in a confocal volume element kept at a fixed position within the sample. In point fluorescence recovery after photobleaching (*pFRAP*), the initial fluorescence signal is recorded, followed by a bleach with a short laser intensity burst, and measurement of the fluorescence signal recovery. For point continuous fluorescence photobleaching (*pCP*), partial bleaching occurs via continuous illumination with moderate intensity. The decay of the fluorescence signal is recorded. In point fluorescence correlation spectroscopy (*pFCS*), the intensity fluctuations of the fluorescence signal are measured. **b** Scanning FCS methods. In *line/circular sFCS*, the focus volume is moved along a line or a circle (scan progress is depicted by a color gradient). The fluorescence signal at corresponding points is sequentially detected. Scanning is repeated and averaged to improve the signal-to-noise ratio. *STICS/RICS* (spatio-temporal/raster image correlation spectroscopy) uses sequential illumination of the sample by confocal point scanning. The correlation of intensity fluctuations between different points of the optical section is calculated. *RICS* and *STICS* differ with respect to the data analysis and mobility information retrieved (see text for details). **c** FCS methods with parallel data acquisition. For multifocal FCS (*mfFCS*) simultaneous illumination at multiple foci is conducted with parallel data acquisition at these sites. Two experimental setups have been implemented to date: the double focus FCS (*dfFCS*) and the spinning disk confocal microscopy-FCS (*SDCM-FCS*). The technique of 1-dimensional FCS (*1D-FCS*) is based on a line-shaped excitation and detection focus volume for parallel measurements of fluorescence intensity fluctuations at all points detected along the line. In 2-dimensional FCS (*2D-FCS*) either a TIRF setup or a single light sheet is used for excitation of an optical section. Fluorescence intensity fluctuations are recorded on the 2D pixel array of an EMCCD detector

librium state in order to determine diffusion properties and interactions (Elson and Magde 1974; Magde et al. 1974; Wachsmuth and Weissbart 2007). Concentration fluctuations can be measured at concentrations of fluorescently labeled proteins in the nM to μM range. In a point FCS (pFCS) experiment, the focus of a confocal laser illumination and fluorescence detection system like that of a CLSM defines a small observation volume. As for pFRAP and point CP, it is fixed at a position of interest (Fig. 1a). Due to their diffusion, fluorescently labeled molecules can enter and leave the focus, resulting in signal fluctuations at the detector. The amplitude of the fluctuations is related to the number of molecules, whereas the characteristic dwell time inside the focal volume is determined from the decay of the curve. Thus, appropriate models for the source of fluctuations and the characteristic shape of

the focal volume allow for deriving concentrations and diffusion coefficients as well as for distinguishing freely diffusing proteins from proteins bound to large complexes or cellular structures. FCS measurements at different cellular locations (typically of 10–60 s at each locus) can be performed sequentially to look for correlations between mobility and interactions with cellular structures (Dross et al. 2009; Müller et al. 2009; Schmidt et al. 2009). In principle, this can be done at enough positions to derive a mobility map with the caveat that during the data acquisition period cell dynamics usually become significant. Depending on mobility and brightness of the particle the acquisition time for a correlation analysis can be reduced to some seconds or even tens of milliseconds to increase the number of cellular regions that are sampled (Roth et al. 2007). By extending the FCS setup to a two-color system and by labeling potentially interacting proteins with two spectrally distinct fluorophores, fluorescence cross-correlation spectroscopy provides a highly sensitive readout for bimolecular interactions (Ricka and Binkert 1989; Rippe 2000; Schwillie et al. 1997).

Point scanning correlation spectroscopy methods

Scanning fluorescence correlation spectroscopy The scanning FCS (sFCS) technique refers to a variety of FCS methods, in which the focus is scanned repetitively along a line or a circle (Fig. 1b) (Berland et al. 1996; Petersen 1986; Petrusek and Schwillie 2008; Weissman et al. 1976). By moving the observation volume, very slow diffusion and transport processes can be studied, extending the range of diffusion coefficients accessible with FCS to lower values around $10^{-3} \mu\text{m}^2 \text{ s}^{-1}$ (Ries and Schwillie 2006). Photobleaching effects are alleviated and statistical accuracy is improved due to short time lags between sequential measurements at multiple points within the sample. With sFCS it is possible to measure diffusion coefficients, flow direction, and speed as well as the position of immobilized particles (Skinner et al. 2005). Another difficulty in pFCS is the correct determination of the focal volume to calculate the diffusion coefficient and the concentration exactly. Using circular scanning FCS with a known scan radius as a spatial measure or two-foci cross-correlation analysis of two alternately scanned parallel lines, sFCS becomes insensitive to disturbances affecting the size of the focal volume (Petrusek and

Table 1 Experimental parameters of fluorescence fluctuation methods

Method	Spatial resolution ^a	Temporal resolution	D ($\mu\text{m}^2 \text{s}^{-1}$)	Concentration	References
pCP	200×200×600 nm	ms–s	–	nM–mM	Peters et al. 1981; Wachsmuth et al. 2003
pFRAP	200×200×600 nm	100 μs –s	<10	nM–mM	Axelrod et al. 1976; Edidin et al. 1976; Peters et al. 1974; Schmidt et al. 2009
pFCS	200×200×600 nm	μs –s	>0.1	pM– μM	Elson and Magde 1974; Magde et al. 1974
sFCS	$\sim 1 \times 0.2 \times 0.6 \mu\text{m}$	ms	>0.001	pM– μM	Digman et al. 2005a; Ries and Schwille 2006; Ruan et al. 2004
TICS	$\sim 1 \times 1 \times 0.6 \mu\text{m}$	s	~ 1	nM– μM	Kolin and Wiseman 2007; Srivastava and Petersen 1996; Wiseman et al. 2000
STICS	$\sim 1 \times 1 \times 0.6 \mu\text{m}$	ms–s	>0.001	nM– μM	Hebert et al. 2005; Wiseman et al. 2004
RICS	$\sim 1 \times 1 \times 0.6 \mu\text{m}$	μs –s	>0.001	nM– μM	Digman et al. 2005a, b
mfFCS	200×200×600 nm	μs –s	>0.001	pM– μM	Brinkmeier et al. 1997; Dertinger et al. 2007; Dittrich and Schwille 2002; Needleman et al. 2009; Sisan et al. 2006
1D-FCS	200×380×700 nm	15 μs	>0.1	nM– μM	Carrero et al. 2003
2D-FCS	400×400×400 nm	40 μs	>0.1	nM– μM	Capoulade et al. 2010; Kannan et al. 2007; Wohland et al. 2010

^aThe point CP, FRAP, and FCS as well as the dfFCS experiments are conducted with a confocal microscopy setup with a resolution of about 200×200×600 nm under optimal conditions. sFCS and TICS/STICS/RICS are based on point scanning with the same resolution. However, in practice averaging along the scan line as in sFCS or of an area (raster ICS methods) is conducted to improve the accuracy. In 1D- and 2D-FCS, the lateral resolution is somewhat reduced because a different optical setup is used

Schwille 2008; Ries and Schwille 2006), and offers an approach to directly detect barriers and other deviations from free diffusion (Digman and Gratton 2009).

Image correlation spectroscopy methods (TICS, STICS, and RICS) A variety of image correlation spectroscopy (ICS) methods exist that extract information like densities and concentrations, aggregation, diffusion coefficients, velocities and flow directions as well as interaction parameters from image series acquired with standard fluorescence confocal laser scanning microscopes (Fig. 1b) (Kolin and Wiseman 2007; Petersen et al. 1993). In general, temporal and/or spatial correlations are computed from fluorescence intensity fluctuations of image pixels. By averaging over cellular areas, a larger number of molecules per frame is sampled and thus better statistics are obtained, albeit at the cost of spatial resolution: ICS can be performed on μm^2 regions, but the larger the region, the more accurate the results. As a mathematical image-processing method, ICS is based on the calculation of the spatial autocorrelation function (SCF) from intensities recorded at each pixel and

fitting with 2D Gaussian functions to extract parameters of interest. From spatial ICS, cluster densities and aggregation states can be determined. To extract molecular dynamics from CLSM images the temporal correlation function of a time series of images is calculated and fitted to an analytical decay model describing the molecular transport (temporal image correlation spectroscopy (TICS)) (Kolin and Wiseman 2007; Srivastava and Petersen 1996; Wiseman et al. 2000). The amplitude and the decay shape of the temporal correlation function describe the particle number as well as the rate (diffusion/transport coefficient) and the mode of the underlying transport process (free/obstructed/confined diffusion, directed movement). Additionally, the percentage of immobilized molecules can be calculated. The time resolution of TICS is limited to the imaging rate of the microscope and diffusion faster than $10^{-2} \mu\text{m}^2 \text{s}^{-1}$ is difficult to resolve. The sequential nature of the scanning process used to acquire a CLSM image defines not only a spatial but also a well-defined temporal sampling of the pixels as defined by the scanner settings. Typical pixel dwell times are in

the μs range, while the time lags between lines are on the ms scale and the times between successive images in the range of s. In raster image correlation spectroscopy (RICS) (Digman et al. 2005a, b), two-dimensional SCFs of the CLSM images are computed that contain contributions from both the scanning process and from the diffusion process, which allows to derive diffusion coefficients up to $\sim 100 \mu\text{m}^2\text{s}^{-1}$. It is essential to correct the data for immobile or slowly mobile components that tend to mask the correlations arising from rapidly diffusing molecules. A critical parameter in RICS is the scan velocity, which has to be chosen in an appropriate relation to particle mobility (Digman et al. 2005a; Kolin and Wiseman 2007). This limitation can be overcome by using a broad range of scan velocities (Gröner et al. 2010).

While TICS and RICS enable the calculation of diffusion or flow constants, the direction of (rather slow) movements can be determined by a complete spatial and temporal, i.e., frame-to-frame, image correlation analysis (spatio-temporal image correlation spectroscopy (STICS)) (Hebert et al. 2005). Here, the resulting peaks of the 2D autocorrelation functions broaden but remain centered owing to diffusion, whereas directional flow shifts the peaks towards the flow direction without changing their shape. Similar to RICS, data must be corrected for immobile and slowly diffusing molecules to get accurate flow data. All image correlation methods depend on an analysis of areas at least in the range of micrometer squared, but larger sections ensure a higher accuracy of the data, where possibly many frames should be taken and averaged to improve statistics. Nevertheless, the analysis of certain regions within the cell allows for calculating maps of concentrations, diffusion and flow parameters and—using STICS—for assembling vector maps illustrating flow velocity and direction.

Multifocal FCS with parallel data acquisition and mobility mapping

Multifocal FCS Shape and size of the focal volume, i.e. of the point spread function of the optical setup, are quite sensitive to parameters like coverglass thickness, refractive index mismatch of sample, glass and immersion medium or heterogeneity of the cellular interior. This may affect the calculation of diffusion coefficients or

concentrations. These problems are avoided in setups termed dual- or two-focus FCS (dfFCS, 2fFCS) that evaluate the cross-correlation of signals between two distinct detection foci (Fig. 1c) (Brinkmeier et al. 1997; Dertinger et al. 2007; Dittrich and Schwille 2002). A good signal-to-noise ratio is obtained by adjusting the distance of the foci such that the particle flux between the foci is sufficiently high, i.e., for pure diffusion the typical distance between the foci is chosen to be smaller than in the presence of directional flow.

In order to measure at more foci simultaneously, spinning disk microscopes have been used (Needleman et al. 2009; Sisan et al. 2006). They enable measurements inside three-dimensional objects, but their coverage of the sample is still incomplete either in space (when parking the disk) or in time (when rotating the disk). Thus, either a restricted number of points is measured with moderate to high temporal resolution or a complete coverage is obtained with a lower temporal resolution of about 1 ms. Spinning disk microscopes usually employ ultra-sensitive electron-multiplying charge-coupled device (EMCCD) cameras. The recent generation of these detectors has a quantum efficiency of up to 90% that is similar to that of an avalanche photodiode at a good signal-to-noise ratio (Art 2006). This allows for spatially resolved single photon detection on a pixel array.

FCS along a line In a recently introduced optical instrument termed the spatial and temporal fluctuation microscope (STFM), the conventional point-confocal focus volume is elongated in one lateral direction to the optical axis by using cylindrical lenses. Thus, the sample is illuminated along a line. The fluorescence emission is acquired simultaneously at tens or hundreds of pixels arranged continuously on a row of the EMCCD detector array (Fig. 1c) (Heuvelman et al. 2009). A high line acquisition rate, i.e., good time resolution of a few tens of μs was obtained with nearly point-confocal spatial resolution. This allows for auto- and cross-correlation data analysis, with the cross-correlation curves being calculated for spatially separated pixels on the line. The result is a spatially resolved line profile for the diffusion coefficient, the concentration and the anomaly parameter. The STFM can be used for simultaneous multi-position measurements, the determination of flow velocities and directed motion or—in homogeneous samples—for time-effective high-precision measurements by averaging over all positions. In comparison

to single-point FCS, a FCS measurement along a line (1D-FCS) with a typical acquisition time of 60 s at 120 positions would only last 1 min instead of more than 2 h—which would be a prohibitively large time for the observation of typical nuclear dynamics or chromatin structure-affecting processes.

FCS with plane excitation and detection To perform parallel FCS measurements of a complete image plane, total internal reflection fluorescence (TIRF) microscopy was used (Kannan et al. 2007). Illumination in the proximity of the coverglass surface is achieved with an evanescent wave, and fluorescence intensity fluctuations in two dimensions are recorded with an EMCCD. A drawback of TIRF-based FCS with plane excitation and detection (2D-FCS) is that only the plane close to the coverglass can be illuminated and analyzed, making it impossible to study proteins in the nucleus. This limitation does not exist for light sheet-based fluorescence microscopy (LSFM). LSFM is a technique that allows optical sectioning inside three-dimensional objects with good background suppression and reduced photobleaching (Dodt et al. 2007; Huisken et al. 2004). Fluorescence signals of the optical section are recorded with an EMCCD detector. The intensity traces of the pixels are subjected to an auto- and cross-correlation analysis so that a spatially resolved FCS analysis of a complete image plane becomes possible (Fig. 1c). This setup is referred to here as 2D-FCS. It was recently introduced to conduct first mobility measurements of fluorescent beads with ms time resolution (Wohland et al. 2010) and fluorescent proteins with μ s time resolution inside living cells or tissues (Capoulade et al. 2010). Thus, the 2D-FCS approach can provide comprehensive spatial maps of diffusion coefficients or concentrations extracted from up to thousands of correlation curves acquired simultaneously.

Theoretical considerations for analyzing protein mobility data

Brownian motion

The microscopic origin of Brownian motion is the collision with solvent molecules that move randomly due to their thermal energy. This counteracts any

concentration gradient that is actively established within the cell and leads to particle diffusion with random translocations. In the absence of perturbations, diffusing particles explore an area, the so-called mean squared displacement (MSD), which increases linearly with time. The corresponding slope is proportional to the diffusion coefficient. Considering typical diffusion coefficients at physiological temperatures, diffusion can be very fast and efficient for transferring particles to all accessible locations on the scale of a cell nucleus, i.e. a few tens of micrometers and below. For a small inert protein with a typical diffusion coefficient in the range of $20\text{--}25\ \mu\text{m}^2\ \text{s}^{-1}$ at the viscosity of the nucleoplasm it takes less than one second to diffuse across the whole cell nucleus. However, unperturbed diffusion is virtually never observed inside a cell due to several types of interactions, namely binding interactions and collisions with the surrounding environment (Fig. 2).

Binding leads to decreased mobility

Many proteins undergo some sort of binding interactions while they translocate through the cell nucleus. Although core histones and their variants as well as some centromere proteins are stably associated with chromatin for up to an hour or more, most chromatin-interacting proteins bind transiently, i.e., on the time scale from milliseconds to minutes (Hager et al. 2009; Hemmerich et al. 2010; Misteli 2007; Wachsmuth et al. 2008). The trajectory of these proteins can be imagined as sequential “hopping”, i.e., there are periods in which the protein is free and diffuses and periods in which the protein is bound to the rather slowly moving chromatin fiber (Fig. 3). Depending on the temporal distribution of diffusion and immobilization, it is either possible to distinguish a bound and a free fraction of the molecules, or their behavior can be described as effective diffusion where the apparent diffusion coefficient D_{eff} is decreased because the particle is trapped part of the time. The fraction of molecules in the bound state is related to the pseudo-equilibrium constant $K_{\text{eq}}^* = k_{\text{on}}^*/k_{\text{off}} = k_{\text{on}} c_{\text{B}}/k_{\text{off}}$, which includes the free binding site concentration c_{B} and kinetic on and off rates. Thus, the free mobility of the particle described by its diffusion coefficient D is related to its binding properties according to $D_{\text{eff}} = D/(1 + k_{\text{on}}^*/k_{\text{off}})$ (Sprague et al. 2004). If the particle interacts transiently with

different binding sites with similar dissociation rates, the particle's motion still follows a normal diffusion process. However, if binding occurs at many different binding sites with a sufficiently broad distribution of interaction rates, mobility follows a continuous time random walk (Blumen 1983). This is referred to as anomalous diffusion or subdiffusion (Saxton 1996). Accordingly, the MSD of the particle over time is no longer linear as for free diffusion but shows reduced diffusion distances that can be described by a power law. The corresponding exponent, the anomaly parameter α , is smaller than 1 for anomalous diffusion caused by binding interactions as described above. In practical terms, anomalous diffusion means that the effective diffusion coefficient depends on the length or time scale. For $\alpha < 1$ the diffusion coefficient decreases on larger scales, i.e., the transport over longer distances is slower than expected. Thus, diffusion coefficients of an anomalous diffusion process measured experimentally on different length scales, e.g. by using FCS, dfFCS or FRAP, do not necessarily yield the same value.

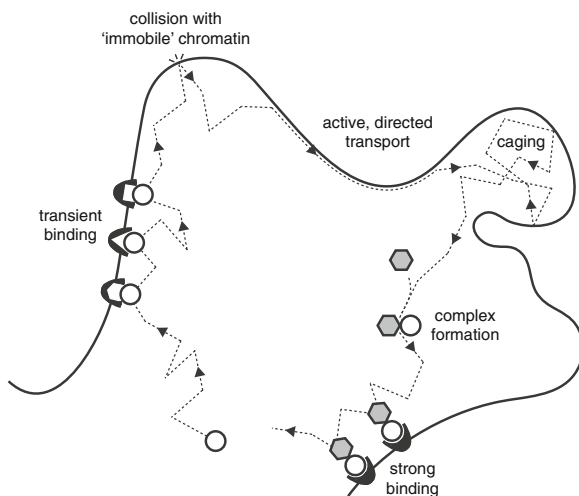


Fig. 2 Diffusion modes and mobilities. Protein mobility in the context of the chromatin environment is influenced by several microscopic phenomena like interactions with immobile binding sites of different affinities, complex formation with mobile factors, collisions with the chromatin fiber or caging inside chromatin loops. While specific binding and complex formation lead to a reduced diffusion coefficient, collisions with immobile obstacles as well as heterogeneous residence times at binding sites with different affinities result in anomalous diffusion behavior (Saxton 1994; Saxton 1996)

Volume exclusion and collisions lead to decreased mobility

A large part of the cell nucleus is occupied by chromatin. The average nucleosome concentration in mammalian cells is 0.14 mM (Weidemann et al. 2003), and the equivalent of 18–19 mgml⁻¹ DNA yields a typical nuclear volume of 0.4 picoliter or a radius of ~4.5 μm ((Zeskind et al. 2007) and references therein). In more densely packed heterochromatin, nucleosome concentrations of 0.2–0.3 mM up to 0.4–0.5 mM are observed (Görisch et al. 2005a; Weidemann et al. 2003). During interphase, particles up to ~20 nm in size experience no restrictions with respect to their nuclear distribution within the 200–300 nm diffraction limit of light microscopy, while larger particles are progressively excluded from dense chromatin regions (Görisch et al. 2005b; Grunwald et al. 2008; Pack et al. 2006; Verschure et al. 2003). At sizes around 100 nm they are completely excluded from the chromatin network (Görisch et al. 2003; Tseng et al. 2004). Thus, exclusion effects can lead to locally increased accumulations of larger proteins or complexes, potentially causing an effective attraction or a spatial confinement or caging (Fig. 2). It should be noted that a particle size of 20 nm would correspond to protein complexes in the MDa range. Thus, at least on the 200–300 nm scale routinely accessible for diffraction-limited resolution imaging of living cells, essentially all parts of chromatin are accessible to protein factors. However, in the presence of a large amount of immobile obstacles, as it is the case in the chromatin environment, collisions affect the mobility, allowing a particle to “sense” its environment and the corresponding geometry. Similar to binding sites with a broad distribution of dissociation rates, this results in anomalous diffusion behavior due to the presence of obstacles, which can be distributed randomly or fractally (Saxton 1994, 1996). In consequence, virtually all proteins in the cell nucleus display anomalous diffusion at least on a certain length scale.

Microscopic origin and macroscopic readout

The analysis of protein mobility and the dissection of the different contributions listed above require a careful experimental analysis (Mueller et al. 2010). To determine whether a diffusion process is anoma-


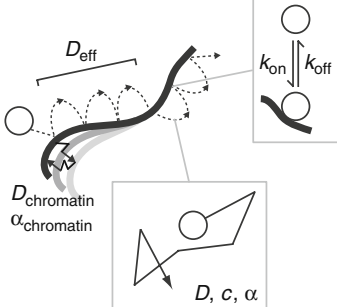
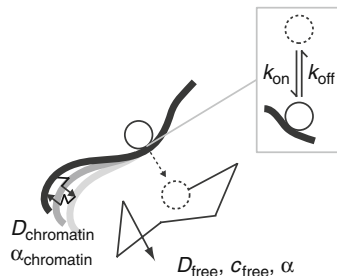
Microscopic event	Observables
<p>diffusion without binding</p>  <p>D, c, α</p>	<p>diffusion coefficient D anomaly parameter α particle concentration c</p> <p>CP: - FCS: D, c, α FRAP: D</p>
<p>transient chromatin-binding</p>  <p>$D_{\text{eff}}, D_{\text{chromatin}}, \alpha_{\text{chromatin}}, k_{\text{on}}, k_{\text{off}}, c_{\text{B}}, c$</p> <p>$D, c, \alpha$</p>	<p>diffusion coefficients $D, D_{\text{eff}}, D_{\text{chromatin}}$ anomaly parameters $\alpha, \alpha_{\text{chromatin}}$ association/dissociation rate $k_{\text{on}}/k_{\text{off}}$ binding site concentration c_{B} particle concentration c</p> <p>CP: - (large k_{off}) k_{off} (medium k_{off})</p> <p>FCS: $D_{\text{eff}}, c, \alpha, D_{\text{chromatin}}, \alpha_{\text{chromatin}}$</p> <p>FRAP: D_{eff} (large $c_{\text{B}} \cdot k_{\text{on}}$) $D, c_{\text{B}} \cdot k_{\text{on}}, k_{\text{off}}$ (medium $c_{\text{B}} \cdot k_{\text{on}}$)</p>
<p>strong chromatin-binding</p>  <p>$D_{\text{chromatin}}, \alpha_{\text{chromatin}}, D_{\text{free}}, c_{\text{free}}, \alpha$</p> <p>$k_{\text{on}}, k_{\text{off}}$</p>	<p>diffusion coefficient D anomaly parameter α dissociation rate k_{off} immobile fraction $immo$ free particle concentration c_{free}</p> <p>CP: k_{off} FCS: $D, c_{\text{free}}, \alpha$ FRAP: $k_{\text{off}}, immo$</p>

Fig. 3 Integrative analysis of the mobility of chromatin-interacting proteins. Different observables are experimentally accessible depending on the type of binding interactions. (1) Diffusion without binding (*upper row*): the diffusion coefficient can be determined by FRAP or FCS (or other types of correlation spectroscopy). The anomaly parameter is typically obtained by FCS or from the comparison between values for the diffusion coefficients on different length scales. (2) Transient chromatin binding (*middle row*): an effective diffusion coefficient reflecting the binding contributions is usually measured by FRAP or FCS analyses. If the binding reaction is

slow enough, the individual rate constants can be extracted using FRAP or CP. Motion of the chromatin fiber (*gray shading*) decorated with continuously exchanging labeled particles leads to a slow component in FCS experiments. (3) Strong chromatin binding (*bottom row*): a free and a bound pool of particles can be distinguished (*solid and dashed lines*); FCS yields the diffusion coefficient and the anomaly parameter of the free pool. FRAP and CP yield the bound and immobile fractions as well as dissociation constants characterizing the binding reaction

lous, a simple FCS measurement is usually enough, yielding the diffusion coefficient on the length scale of the confocal microscope's resolution and the anomaly parameter α (Fig. 3). To verify the FCS data in the presence of multiple mobility populations, measurements on different length scales are instructive (Mueller et al. 2010; Müller et al. 2009).

However, distinguishing between the different origins of anomalous diffusion is challenging, and it is noted that FCS experiments or MSD measurements alone are not sufficient but have to be supported by other observables (Condamin et al. 2008).

The analysis of immobilization and slow binding reactions is a strength of FRAP, since the recovery

curve encodes information about the immobile fraction and the dissociation rate for slow binding processes. However, fast binding events on the time scale of the microscope's acquisition rate or below the diffusion time scale cannot be resolved. A number of more or less explicit expressions for the intensity recovering over time have been reported (Axelrod et al. 1976; Calapez et al. 2002; Simon et al. 1988; Soumpasis 1983; Yguerabide et al. 1982). For the case that neither diffusion nor binding/immobilization dominate the mobility, a more detailed spatio-temporal description in combination with numerical modeling of the complete reaction-diffusion scheme is necessary for the correct interpretation of the data (Beaudouin et al. 2006; Carrero et al. 2003; Mueller et al. 2010; Sprague et al. 2004). Moreover, anomalous diffusion is usually not taken into consideration for the evaluation of FRAP data although the resulting long-tail kinetics can feign slowly diffusing or transiently bound components and has been theoretically considered (Lubelski and Klafter 2008; Nagle 1992; Saxton 2001).

In general, careful evaluation of the data in terms of the number of free parameters is necessary to avoid overinterpretation of the experimental FRAP data. If binding processes do not occur on well-separated time scales, they usually cannot be extracted from the FRAP curve. Thus, a combination of different fluorescence fluctuation microscopy-based techniques is required for accurate determination of interaction parameters (Mueller et al. 2010; Müller et al. 2009) (Fig. 3).

Analysis of chromatin interactions of heterochromatin protein 1

As discussed previously, most chromatin-interacting proteins are surprisingly mobile. Only a few structurally relevant proteins such as the core histones, some centromere proteins and cohesins are stably integrated into chromatin with typical residence times in the range of hours (Hager et al. 2009; Hemmerich et al. 2010; Misteli 2007; Wachsmuth et al. 2008). In contrast, architectural chromatin proteins like linker histone H1, high mobility group proteins, and HP1 have residence times on chromatin that are in the order of only a few seconds to minutes for the majority protein fraction. Here, we summarize find-

ings on heterochromatin protein 1 as a prototypic example for a chromosomal protein that is involved in establishing and maintaining a biologically inactive heterochromatin state with a dependence on a specific set of epigenetic signals (Eissenberg and Reuter 2009; Grewal and Jia 2007). HP1 is present in three very similar isoforms HP1 α , HP1 β and HP1 γ in mice and humans (Hiragami and Festenstein 2005; Kwon and Workman 2008; Maison and Almouzni 2004). It contains an N-terminal chromodomain (CD) that binds preferentially to H3 histone tails that carry the K9me2/3 modification (Fischle et al. 2003; Jacobs and Khorasanizadeh 2002). Since HP1 interacts with the histone methyltransferases Suv3-9h1/2 and Suv4-20h1/2 that induce the characteristic histone modifications of pericentric heterochromatin H3K9me2/3 and H4K20me2/3, it has been proposed that heterochromatin assembly is nucleated by the targeting of HP1 via its CD to H3K9me2/3. Through the interaction of HP1 with Suv3-9h1/2 a feedback loop of HP1 binding-mediated H3K9 methylation could promote HP1 binding to adjacent nucleosomes to both maintain the heterochromatin and propagate it to adjacent regions (Eissenberg and Reuter 2009; Grewal and Jia 2007). This type of interconnection between epigenetic modifications of histone residues with the readout of these marks by specific protein domains is a typical feature of epigenetic networks (Dodd et al. 2007; Schreiber and Bernstein 2002). Accordingly, the formation of pericentric heterochromatin via HP1, Suv3-9h1/2, Suv4-20h1/2 and other proteins can be considered as a prototypic example.

Since the nuclear mobility and chromatin interactions of HP1 have been characterized in a number of FRAP and FCS studies it is also particularly suited to compare different fluorescence bleaching and correlation approaches (Cheutin et al. 2003, 2004; Dialynas et al. 2007; Festenstein et al. 2003; Krouwels et al. 2005; Müller et al. 2009; Schmiedeberg et al. 2004; Souza et al. 2009). Initial mobility studies of HP1 based on the imaging FRAP measurements revealed the high mobility of the protein and the frequent turnover between its chromatin-bound state and the freely mobile state within the nucleoplasm (Cheutin et al. 2003; Festenstein et al. 2003). Subsequent FRAP studies led to a model with at least three mobility states with different on and off rates that were related to the histone H3 methylation state (Cheutin et al.

2004; Schmiedeberg et al. 2004). However, the contribution of diffusion versus binding interactions to the observed mobility was not clearly separated in these studies. For HP1 interactions in the nucleus diffusion is relevant since the time scale to associate with a binding site is similar to the time the protein needs to translocate across a FRAP bleach spot in the μm range. This was accounted for in a recent multiscale reaction-diffusion analysis that applied complementary photobleaching and fluorescence correlation microscopy methods (FRAP, FCS, CP, and FLIP) in mouse fibroblast cells (Müller et al. 2009). Three different binding classes that characterized the inactive or active chromatin state were extracted from a spatially resolved mobility analysis of HP1 α and HP1 β . Furthermore, the results from FRAP, FCS, and CP experiments could be integrated into a consistent description when considering the different temporal and spatial scales of the different types of measurements. The results of various types of HP1 mobility measurements obtained with different methods are summarized in Table 2. The interaction of HP1 with chromatin is expressed in terms of an effective diffusion coefficient D_{eff} that reflects the mobility reduction due to binding events (see “Binding leads to decreased mobility” and Fig. 3). As a reference for the freely mobile state of HP1 a diffusion coefficient of 23–26 $\mu\text{m}^2\text{s}^{-1}$ in the cytoplasm was measured (Table 2). The previous studies based on imaging FRAP measurements yielded half times, diffusion coefficients or on/off rates for HP1 that vary over a large range. Effective diffusion coefficients were calculated to be in the range from 0.003 to 0.43 $\mu\text{m}^2\text{s}^{-1}$ in the less DNA dense euchromatin and from $6 \cdot 10^{-4}$ to 0.49 $\mu\text{m}^2\text{s}^{-1}$ in heterochromatin (Table 2). For each individual study the diffusion coefficients of HP1 in euchromatin and heterochromatin differed significantly. However, when considering all FRAP studies, the smallest and the largest D values covered a large range of two orders of magnitude that is almost identical for eu- and heterochromatin. The large variation of these data might reflect to some extent specific features of the experimental system studied as for example the cell type (yeast, mouse, or human), the HP1 isoform (α , β , or γ), the concentration of the GFP tagged HP1 construct or cell cycle effects. However, differences by a factor of >100 also point to fundamental problems with the integration of results that arise

from the various types of data analysis used (Mueller et al. 2010). It is noted that the available data clearly point to the existence of different binding site classes that reflect the histone H3K9 methylation status (Cheutin et al. 2004; Müller et al. 2009; Schmiedeberg et al. 2004). By relying on imaging-based FRAP as the sole experimental approach the associated binding site heterogeneity is difficult to resolve. A complementary use of photobleaching and correlation experiments is advantageous to characterize transient binding sites by an effective diffusion coefficient

Table 2 Fluctuation microscopy measurements of HP1

Technique	D_{eff} ($\mu\text{m}^2\text{s}^{-1}$)		
	Cytoplasm	Euchromatin	Heterochromatin
FRAP ^a	ND	0.003–0.43	0.0006–0.49
RICS ^b	7 \pm 3	0.2–0.4	0.2–0.4
pFCS	23–26	7.7 \pm 0.8 ^c	3.9 \pm 0.9 ^c
1D-FCS ^d	ND	7.9 \pm 0.8 ^c	3.4 \pm 0.4 ^c
2D-FCS ^d	ND	12 \pm 6 ^c	11 \pm 5 ^c

^aData from different FRAP studies (Cheutin et al. 2003, 2004; Dialynas et al. 2007; Festenstein et al. 2003; Krouwels et al. 2005; Müller et al. 2009; Schmiedeberg et al. 2004; Souza et al. 2009). Effective diffusion coefficients D_{eff} (including also binding contributions) were calculated from half times of recovery or refitting the data taking into account the size of the spot or rectangular bleach geometry (Sprague et al. 2004; Wachsmuth and Weissart 2007). The immobile fractions comprised 0–10% (euchromatin) and 5–30% (heterochromatin) and were determined from 30–150 s measurements. Immobilization over this time period corresponds to kinetic off rates k_{off} below 0.03–0.007 s^{-1} .

^bRICS data are shown in Fig. 4b and were acquired from averaging over the indicated $1.5 \times 1.5 \mu\text{m}^2$ areas. The signal-to-noise ratio precluded a distinction between two components of different mobility as in the FCS experiments. Similar values in the range of 0.3–2 $\mu\text{m}^2\text{s}^{-1}$ were measured in another RICS analysis of HP1 (Hemmerich et al. 2010)

^cData are given for measurements of GFP-HP1 α in the same mouse NIH 3T3 line (Müller et al. 2009). The D_{eff} values refer to the more mobile species determined in a two component analysis, in which the second slower component reflects intensity fluctuations due to chromatin dynamics (Fig. 3). In another study, lower values of $D_{\text{eff}}=0.6\text{--}0.7 \mu\text{m}^2\text{s}^{-1}$ for GFP-HP1 $\alpha/\beta/\gamma$ were derived from a one component fit (Schmiedeberg et al. 2004)

^dThe 1D-FCS data were acquired with the STFM (Fig. 4b) (Heuvelman et al. 2009). For 2D-FCS a newly built instrument was used (Capoulade et al. 2010). For the latter, the relatively large error in D_{eff} precluded a distinction of HP1 α mobility in eu- and heterochromatin

cient and to resolve higher affinity binding in terms of distinct kinetic on/off rates. In terms of comparing mobilities and interactions at different nuclear locations, the development of FCS approaches with parallel “multifocal” data acquisition offers a number of advantages (Fig. 1c). It can provide a more comprehensive spatial picture of mobility and interaction differences, and particle mobilities can be evaluated via the spatial cross-correlation of signals between different loci (Heuvelman et al. 2009). For HP1 a comparison between FRAP, RICS, pFCS, 1D-FCS, and 2D-FCS is made in Table 2 and Fig. 4. Since the

RICS analysis sacrifices spatial resolution to retrieve mobility information a distinction between small eu- and heterochromatin structures becomes difficult. With pFCS and 1D-FCS the apparent diffusion coefficients of HP1 α within eu- and heterochromatin were reliably resolved and similar results were obtained. In the 2D-FCS analysis, the relative large error for the determination of D_{eff} with the current experimental setup precluded a distinction between eu- and heterochromatin. However, it is anticipated that the signal-to-noise ratio can be significantly improved in the future to resolve spatial mobility differences of HP1.

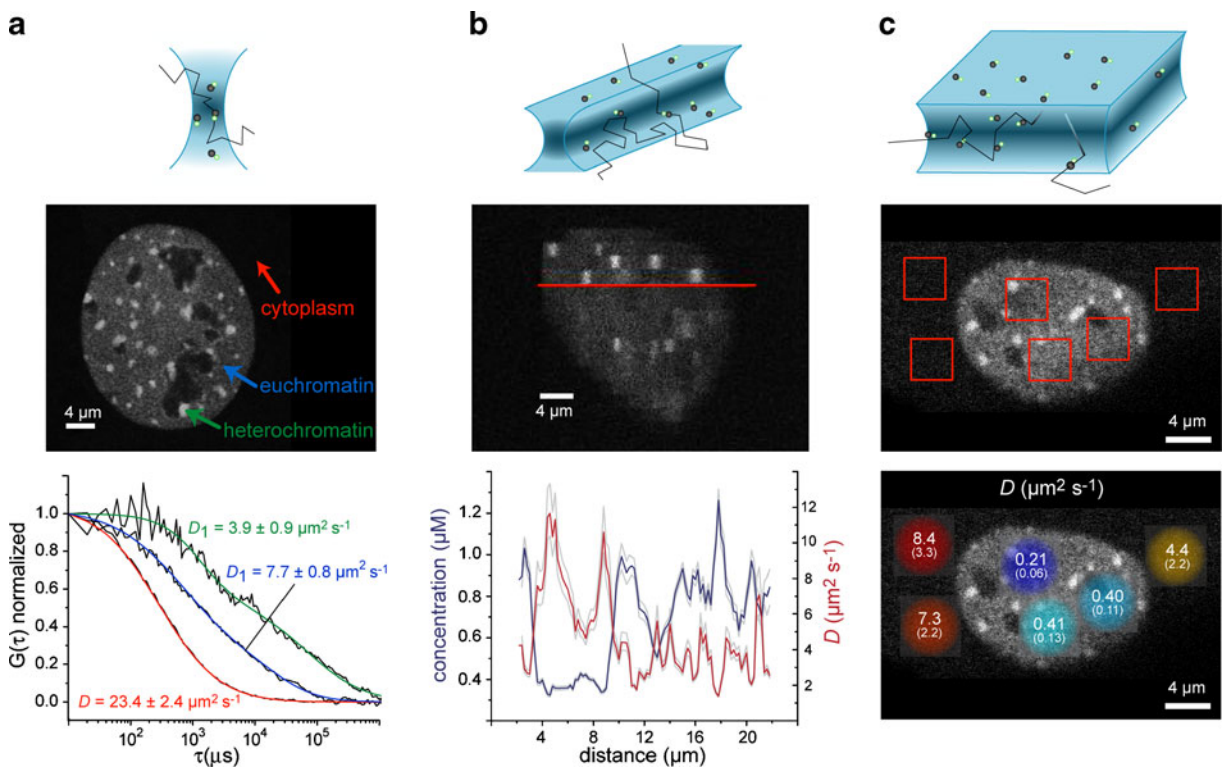


Fig. 4 HP1—point FCS, line FCS and plane scanning FCS. Experimental results of mobility measurements in the cell nucleus. Bright regions are HP1-rich heterochromatin domains. Diffusion coefficients for heterochromatin protein 1 (HP1) were determined with fluorescence microscopy techniques featuring different focus geometries: **a** pFCS. Three single measurements in the cytoplasm, heterochromatin and euchromatin with an acquisition rate of 50 kHz and a total recording time of 60 s. Exemplary autocorrelation functions are illustrated for each region and the diffusion coefficient of the mobile protein fraction is indicated (Müller et al. 2009). **b** 1D-FCS. Data were acquired simultaneously at 100 positions with the STFM with a line rate of 7 kHz and a total recording time of 60 s. The profiles show fluctuations in heterochromatic and euchromatic domains (Heuvelman et al. 2009; Baum, Erdel, Müller,

Wachsmuth and Rippe, unpublished). **c** FCS of a whole image plane. If translocations are sufficiently slow the intensity fluctuations within the optical section can be derived from a time series of confocal images as in RICS. In the example, images were acquired with a range of scanning velocities and subjected to RICS analysis at $1.5 \times 1.5 \mu\text{m}^2$ areas (red squares). The resulting apparent diffusion coefficients and errors were calculated as described elsewhere and are overlaid in appropriate color coding (Gröner et al. 2010). For HP1 the spatial/temporal resolution associated with RICS is not sufficient. This issue can be addressed by using a 2D-FCS setup in which light sheet illumination is combined with detection of intensity fluctuations on an EMCCD (Capoulade et al. 2010; Wohland et al. 2010)

Conclusions

The extension of FCS measurements from a single point to simultaneous measurements of particle mobilities along a line or even in a complete image plane is now becoming technically feasible. This will permit determination of spatially resolved protein mobility maps (Fig. 1, Fig. 4). The current analysis of the temporal dependence of the fluorescence intensity in these experiments is focused on the computation of an auto- or spatial cross-correlation function. This ignores the protein fraction that is immobile on the second time scale as it is bleached by continuous illumination. One possibility to address this shortcoming is to conduct complementary FRAP experiments as reviewed here for the characterization of the mobility of HP1 (Table 2). Usually, imaging-based FRAP experiments are conducted with a resolution in the μm range. However, it is well possible to acquire data with diffraction-limited resolution as implemented in point FRAP or CP experiments (Fig. 1; Table 2) (Delon et al. 2006; Schmidt et al. 2009; Wachsmuth et al. 2003, 2008). Thus, mobility maps obtained from bleaching approaches along a line or a plane can in principle be acquired with the same spatial resolution as the maps generated by intensity correlation analyses (but being potentially limited by the associated reduction of the fluorescence signal to be evaluated). It is noted that for a combined FCS-CP analysis the experimental 1D- or 2D-FCS setups need no further modifications but only an additional analysis of the spatially resolved intensity signal in addition to the computation of the correlation function. The use of these complementary fluorescence fluctuation microscopy approaches in combination with appropriate theoretical descriptions is a powerful approach to dissect protein mobility and interaction parameters in living cells. By deriving chromatin interaction data at different nuclear localizations essential parameters like kinetic on and off rates for different classes of binding sites and concentrations can be determined to develop quantitative models. These will provide insights into the mechanisms that govern the establishment and maintenance of different functional chromatin states as well as other cellular functions.

Acknowledgements This work was supported by the project EpiSys within the BMBF SysTec program. Due to space limitations, many of the relevant primary publications could not be cited. We thank Thomas Höfer for discussions.

References

- Art J (2006) Photon detectors for confocal microscopy. In: Pawley JB (ed) Handbook of biological confocal microscopy. Springer, New York, pp 251–264
- Axelrod D, Koppel DE, Schlessinger J, Elson E, Webb WW (1976) Mobility measurement by analysis of fluorescence photobleaching recovery kinetics. *Biophys J* 16:1055–1069
- Beaudouin J, Mora-Bermúdez F, Klee T, Daigle N, Ellenberg J (2006) Dissecting the contribution of diffusion and interactions to the mobility of nuclear proteins. *Biophys J* 90:1878–1894
- Berland KM, So PT, Chen Y, Mantulin WW, Gratton E (1996) Scanning two-photon fluctuation correlation spectroscopy: particle counting measurements for detection of molecular aggregation. *Biophys J* 71:410–420
- Blumen A, Klafter J, Zumofen G (1983) Recombination in amorphous materials as a continuous-time random-walk problem. *Phys Rev B* 27:3429–3435
- Brinkmeier M, Dorre K, Riebeseel K, Rigler R (1997) Confocal spectroscopy in microstructures. *Biophys Chem* 66:229–239
- Calapez A, Pereira HM, Calado A, Braga J, Rino J, Carvalho C, Tavanetz JP, Wahle E, Rosa AC, Carmo-Fonseca M (2002) The intranuclear mobility of messenger RNA binding proteins is ATP dependent and temperature sensitive. *J Cell Biol* 159:795–805
- Campos EI, Reinberg D (2009) Histones: annotating chromatin. *Annu Rev Genet* 43:559–599
- Capoulade J, Knop M, Wachsmuth M (2010) Spatially Resolved Fluorescence Fluctuation Spectroscopy (FFS) in Living Cells. *Biophys J* 98:761a
- Carrero G, McDonald D, Crawford E, de Vries G, Hendzel MJ (2003) Using FRAP and mathematical modeling to determine the in vivo kinetics of nuclear proteins. *Methods* 29:14–28
- Cheutin T, McNairn AJ, Jenuwein T, Gilbert DM, Singh PB, Misteli T (2003) Maintenance of stable heterochromatin domains by dynamic HP1 binding. *Science* 299:721–725
- Cheutin T, Gorski SA, May KM, Singh PB, Misteli T (2004) In vivo dynamics of Swi6 in yeast: evidence for a stochastic model of heterochromatin. *Mol Cell Biol* 24:3157–3167
- Cole NB, Smith CL, Sciaky N, Terasaki M, Edidin M, Lippincott-Schwartz J (1996) Diffusional mobility of Golgi proteins in membranes of living cells. *Science* 273:797–801
- Condamin S, Tejedor V, Voituriez R, Bénichou O, Klafter J (2008) Probing microscopic origins of confined subdiffusion by first-passage observables. *Proc Natl Acad Sci USA* 105:5675–5680
- Cutts LS, Roberts PA, Adler J, Davies MC, Melia CD (1995) Determination of localized diffusion coefficients in gels using confocal scanning laser microscopy. *J Microscopy* 180:131–139
- Delon A, Usson Y, Derouard J, Biben T, Souchier C (2006) Continuous photobleaching in vesicles and living cells: a measure of diffusion and compartmentation. *Biophys J* 90:2548–2562
- Dertinger T, Pacheco V, von der Hocht I, Hartmann R, Gregor I, Enderlein J (2007) Two-focus fluorescence correlation

- spectroscopy: a new tool for accurate and absolute diffusion measurements. *Chemphyschem* 8:433–443
- Dialynas GK, Terjung S, Brown JP, Aucott RL, Baron-Luhr B, Singh PB, Georgatos SD (2007) Plasticity of HP1 proteins in mammalian cells. *J Cell Sci* 120:3415–3424
- Digman MA, Gratton E (2009) Imaging barriers to diffusion by pair correlation functions. *Biophys J* 97:665–673
- Digman MA, Brown CM, Sengupta P, Wiseman PW, Horwitz AR, Gratton E (2005a) Measuring fast dynamics in solutions and cells with a laser scanning microscope. *Biophys J* 89:1317–1327
- Digman MA, Sengupta P, Wiseman PW, Brown CM, Horwitz AR, Gratton E (2005b) Fluctuation correlation spectroscopy with a laser-scanning microscope: exploiting the hidden time structure. *Biophys J* 88:L33–L36
- Dittrich PS, Schwille P (2002) Spatial two-photon fluorescence cross-correlation spectroscopy for controlling molecular transport in microfluidic structures. *Anal Chem* 74:4472–4479
- Dodd IB, Micheelsen MA, Sneppen K, Thon G (2007) Theoretical analysis of epigenetic cell memory by nucleosome modification. *Cell* 129:813–822
- Dotz H-U, Leischner U, Schierloh A, Jährling N, Mauch CP, Deininger K, Deussing JM, Eder M, Zieglgänsberger W, Becker K (2007) Ultramicroscopy: three-dimensional visualization of neuronal networks in the whole mouse brain. *Nat Meth* 4:331–336
- Dross N, Spriet C, Zwerger M, Muller G, Waldeck W, Langowski J (2009) Mapping eGFP oligomer mobility in living cell nuclei. *PLoS ONE* 4:e5041
- Edidin M, Zagayansky Y, Lardner TJ (1976) Measurement of membrane protein lateral diffusion in single cells. *Science* 191:466–468
- Eisenberg JC, Reuter G (2009) Cellular mechanism for targeting heterochromatin formation in *Drosophila*. *Int Rev Cell Mol Biol* 273:1–47
- Elson EL, Magde D (1974) Fluorescence correlation spectroscopy I. Conceptual basis and theory. *Biopolymers* 13:1–27
- Festenstein R, Pagakis SN, Hiragami K, Lyon D, Verreault A, Sekkali B, Kiousis D (2003) Modulation of heterochromatin protein 1 dynamics in primary Mammalian cells. *Science* 299:719–721
- Fischle W, Wang Y, Jacobs SA, Kim Y, Allis CD, Khorasanizadeh S (2003) Molecular basis for the discrimination of repressive methyl-lysine marks in histone H3 by Polycomb and HP1 chromodomains. *Genes Dev* 17:1870–1881
- Görisch SM, Richter K, Scheuermann MO, Herrmann H, Lichter P (2003) Diffusion-limited compartmentalization of mammalian cell nuclei assessed by microinjected macromolecules. *Exp Cell Res* 289:282–294
- Görisch SM, Lichter P, Rippe K (2005a) Mobility of multi-subunit complexes in the nucleus: chromatin dynamics and accessibility of nuclear subcompartments. *Histochem Cell Biol* 123:217–228
- Görisch SM, Wachsmuth M, Fejes Tóth K, Lichter P, Rippe K (2005b) Histone acetylation increases chromatin accessibility. *J Cell Sci* 118:5825–5834
- Grewal SI, Jia S (2007) Heterochromatin revisited. *Nat Rev Genet* 8:35–46
- Gröner N, Capoulade J, Cremer C, Wachsmuth M (2010) Measuring and imaging diffusion with multiple scan speed image correlation spectroscopy. *Optics Express* (in press)
- Grunwald D, Martin RM, Buschmann V, Bazett-Jones DP, Leonhardt H, Kubitschek U, Cardoso MC (2008) Probing intranuclear environments at the single-molecule level. *Biophys J* 94:2847–2858
- Hager GL, McNally JG, Misteli T (2009) Transcription dynamics. *Mol Cell* 35:741–753
- Haustein E, Schwille P (2007) Fluorescence correlation spectroscopy: novel variations of an established technique. *Annu Rev Biophys Biomol Struct* 36:151–169
- Hayashi-Takanaka Y, Yamagata K, Nozaki N, Kimura H (2009) Visualizing histone modifications in living cells: spatiotemporal dynamics of H3 phosphorylation during interphase. *J Cell Biol* 187:781–790
- Hebert B, Costantino S, Wiseman PW (2005) Spatiotemporal image correlation spectroscopy (STICS) theory, verification, and application to protein velocity mapping in living CHO cells. *Biophys J* 88:3601–3614
- Hemmerich P, Schmiedeberg L, Diekmann S (2010) Dynamic as well as stable protein interactions contribute to genome function and maintenance. *Chromosome Res* (in this issue)
- Heuvelman G, Erdel F, Wachsmuth M, Rippe K (2009) Analysis of protein mobilities and interactions in living cells by multifocal fluorescence fluctuation microscopy. *Eur Biophys J* 38:813–828
- Hiragami K, Festenstein R (2005) Heterochromatin protein 1: a pervasive controlling influence. *Cell Mol Life Sci* 62:2711–2726
- Huisken J, Swoger J, Del Bene F, Wittbrodt J, Stelzer EH (2004) Optical sectioning deep inside live embryos by selective plane illumination microscopy. *Science* 305:1007–1009
- Jacobs SA, Khorasanizadeh S (2002) Structure of HP1 chromodomain bound to a lysine 9-methylated histone H3 tail. *Science* 295:2080–2083
- Kannan B, Guo L, Sudhaharan T, Ahmed S, Maruyama I, Wohland T (2007) Spatially resolved total internal reflection fluorescence correlation microscopy using an electron multiplying charge-coupled device camera. *Anal Chem* 79:4463–4470
- Kimura H, Hayashi-Takanaka Y, Yamagata K (2010) Visualization of DNA methylation and histone modifications in living cells. *Curr Opin Cell Biol* 22:412–418
- Kolin DL, Wiseman PW (2007) Advances in image correlation spectroscopy: measuring number densities, aggregation states, and dynamics of fluorescently labeled macromolecules in cells. *Cell Biochem Biophys* 49:141–164
- Krouwels IM, Wiesmeijer K, Abraham TE, Molenaar C, Verwoerd NP, Tanke HJ, Dirks RW (2005) A glue for heterochromatin maintenance: stable SUV39H1 binding to heterochromatin is reinforced by the SET domain. *J Cell Biol* 170:537–549
- Kwon SH, Workman JL (2008) The heterochromatin protein 1 (HP1) family: put away a bias toward HP1. *Mol Cells* 26:217–227
- Lee BM, Mahadevan LC (2009) Stability of histone modifications across mammalian genomes: implications for ‘epigenetic’ marking. *J Cell Biochem* 108:22–34
- Li GW, Elf J (2009) Single molecule approaches to transcription factor kinetics in living cells. *FEBS Lett* 583:3979–3983

- Lubelski A, Klafter J (2008) Fluorescence recovery after photobleaching: the case of anomalous diffusion. *Biophys J* 94:4646–4653
- Magde D, Elson EL, Webb WW (1974) Fluorescence correlation spectroscopy II. An experimental realization. *Biopolymers* 13:29–61
- Maison C, Almouzni G (2004) HP1 and the dynamics of heterochromatin maintenance. *Nat Rev Mol Cell Biol* 5:296–304
- McBryant SJ, Adams VH, Hansen JC (2006) Chromatin architectural proteins. *Chromosome Res* 14:39–51
- Misteli T (2007) Beyond the sequence: cellular organization of genome function. *Cell* 128:787–800
- Mueller F, Mazza D, Stasevich TJ, McNally JG (2010) FRAP and kinetic modeling in the analysis of nuclear protein dynamics: what do we really know? *Curr Opin Cell Biol* 22:403–411
- Müller KP, Erdel F, Caudron-Herger M, Marth C, Fodor BD, Richter M, Scaranaro M, Beaudouin J, Wachsmuth M, Rippe K (2009) Multiscale analysis of dynamics and interactions of heterochromatin protein 1 by fluorescence fluctuation microscopy. *Biophys J* 97:2876–2885
- Nagle JF (1992) Long tail kinetics in biophysics? *Biophys J* 63:366–370
- Needleman DJ, Xu Y, Mitchison TJ (2009) Pin-hole array correlation imaging: highly parallel fluorescence correlation spectroscopy. *Biophys J* 96:5050–5059
- Pack C, Saito K, Tamura M, Kinjo M (2006) Microenvironment and effect of energy depletion in the nucleus analyzed by mobility of multiple oligomeric EGFPs. *Biophys J* 91:3921–3936
- Peters R, Peters J, Tews KH, Bahr W (1974) A micro-fluorimetric study of translational diffusion in erythrocyte membranes. *Biochim Biophys Acta* 367:282–294
- Peters R, Brüngrer A, Schulten K (1981) Continuous fluorescence microphotolysis: A sensitive method for study of diffusion processes in single cells. *Proc Natl Acad Sci USA* 78:962–966
- Petersen NO (1986) Scanning fluorescence correlation spectroscopy I. Theory and simulation of aggregation measurements. *Biophys J* 49:809–815
- Petersen NO, Hoddellius PL, Wiseman PW, Seger O, Magnusson KE (1993) Quantitation of membrane receptor distributions by image correlation spectroscopy: concept and application. *Biophys J* 65:1135–1146
- Petrásek Z, Schwillle P (2008) Precise measurement of diffusion coefficients using scanning fluorescence correlation spectroscopy. *Biophys J* 94:1437–1448
- Ricka J, Binkert T (1989) Direct measurement of a distinct correlation function by fluorescence cross correlation. *Phys Rev A* 39:2646–2652
- Ries J, Schwillle P (2006) Studying slow membrane dynamics with continuous wave scanning fluorescence correlation spectroscopy. *Biophys J* 91:1915–1924
- Rippe K (2000) Simultaneous binding of two DNA duplexes to the NtrC-enhancer complex studied by two-color fluorescence cross-correlation spectroscopy. *Biochemistry* 39:2131–2139
- Roth CM, Heinlein PI, Heilemann M, Herten DP (2007) Imaging diffusion in living cells using time-correlated single-photon counting. *Anal Chem* 79:7340–7345
- Ruan Q, Cheng MA, Levi M, Gratton E, Mantulin WW (2004) Spatial-temporal studies of membrane dynamics: scanning fluorescence correlation spectroscopy (SFCS). *Biophys J* 87:1260–1267
- Sasaki K, Ito T, Nishino N, Khochbin S, Yoshida M (2009) Real-time imaging of histone H4 hyperacetylation in living cells. *Proc Natl Acad Sci USA* 106:16257–16262
- Saxton MJ (1994) Anomalous diffusion due to obstacles: a Monte Carlo study. *Biophys J* 66:394–401
- Saxton MJ (1996) Anomalous diffusion due to binding: a Monte Carlo study. *Biophys J* 70:1250–1262
- Saxton MJ (2001) Anomalous subdiffusion in fluorescence photobleaching recovery: a Monte Carlo study. *Biophys J* 81:2226–2240
- Schmidt U, Im K-B, Benzing C, Janjetovic S, Rippe K, Lichter P, Wachsmuth M (2009) Assembly and mobility of exon-exon junction complexes in living cells. *RNA* 15:862–876
- Schmiedeberg L, Weissart K, Diekmann S, Meyer Zu Hoerste G, Hemmerich P (2004) High- and low-mobility populations of HP1 in heterochromatin of mammalian cells. *Mol Biol Cell* 15:2819–2833
- Schreiber SL, Bernstein BE (2002) Signaling network model of chromatin. *Cell* 111:771–778
- Schwillle P, Meyer-Almes FJ, Rigler R (1997) Dual-color fluorescence cross-correlation spectroscopy for multicomponent diffusional analysis in solution. *Biophys J* 72:1878–1886
- Siebrasse JP, Grunwald D, Kubitschek U (2007) Single-molecule tracking in eukaryotic cell nuclei. *Anal Bioanal Chem* 387:41–44
- Simon JR, Gough A, Urbanik E, Wang F, Lanni F, Ware BR, Taylor DL (1988) Analysis of rhodamine and fluorescein-labeled F-actin diffusion in vitro by fluorescence photobleaching recovery. *Biophys J* 54:801–815
- Sisan DR, Arevalo R, Graves C, McAllister R, Urbach JS (2006) Spatially resolved fluorescence correlation spectroscopy using a spinning disk confocal microscope. *Biophys J* 91:4241–4252
- Skinner JP, Chen Y, Muller JD (2005) Position-sensitive scanning fluorescence correlation spectroscopy. *Biophys J* 89:1288–1301
- Soumpasis DM (1983) Theoretical analysis of fluorescence photobleaching recovery experiments. *Biophys J* 41:95–97
- Souza PP, Volkel P, Trinell D, Vandamme J, Rosnoblet C, Heliot L, Angrand PO (2009) The histone methyltransferase SUV420H2 and Heterochromatin Proteins HP1 interact but show different dynamic behaviours. *BMC Cell Biol* 10:41
- Sprague BL, Pego RL, Stavreva DA, McNally JG (2004) Analysis of binding reactions by fluorescence recovery after photobleaching. *Biophys J* 86:3473–3495
- Srivastava M, Petersen NO (1996) Image cross-correlation spectroscopy: a new experimental biophysical approach to measurements of slow diffusion of fluorescent molecules. *Meth Cell Sci* 18:47–54
- Taverna SD, Li H, Ruthenburg AJ, Allis CD, Patel DJ (2007) How chromatin-binding modules interpret histone modifications: lessons from professional pocket pickers. *Nat Struct Mol Biol* 14:1025–1040
- Tseng Y, Lee JS, Kole TP, Jiang I, Wirtz D (2004) Micro-organization and visco-elasticity of the interphase nucleus

- revealed by particle nanotracking. *J Cell Sci* 117:2159–2167
- van Holde KE (1989) *Chromatin*. Springer, Heidelberg
- Verschure PJ, van der Kraan I, Manders EM, Hoogstraten D, Houtsmuller AB, van Driel R (2003) Condensed chromatin domains in the mammalian nucleus are accessible to large macromolecules. *EMBO Rep* 4:861–866
- Wachsmuth M, Weisshart K (2007) Fluorescence photobleaching and fluorescence correlation spectroscopy: two complementary technologies to study molecular dynamics in living cells. In: Shorte SL, Frischknecht F (eds) *Imaging Cellular and Molecular Biological Functions*. Springer Verlag, Heidelberg
- Wachsmuth M, Weidemann T, Muller G, Hoffmann-Rohrer UW, Knoch TA, Waldeck W, Langowski J (2003) Analyzing intracellular binding and diffusion with continuous fluorescence photobleaching. *Biophys J* 84:3353–3363
- Wachsmuth M, Caudron-Herger M, Rippe K (2008) Genome organization: Balancing stability and plasticity. *Biochim Biophys Acta* 1783:2061–2079
- Wang Y, Shyy JY-J, Chien S (2008) Fluorescence proteins, live-cell imaging, and mechanobiology: seeing is believing. *Annu Rev Biomed Eng* 10:1–38
- Weidemann T, Wachsmuth M, Knoch TA, Muller G, Waldeck W, Langowski J (2003) Counting nucleosomes in living cells with a combination of fluorescence correlation spectroscopy and confocal imaging. *J Mol Biol* 334:229–240
- Weissman MB, Schindler H, Feher G (1976) Determination of molecular weights by fluctuation spectroscopy: Application to DNA. *Proc Natl Acad Sci USA* 73: 2776–2780
- Wiseman PW, Squier JA, Ellisman MH, Wilson KR (2000) Two-photon image correlation spectroscopy and image cross-correlation spectroscopy. *J Microsc* 200:14–25
- Wiseman PW, Brown CM, Webb DJ, Hebert B, Johnson NL, Squier JA, Ellisman MH, Horwitz AF (2004) Spatial mapping of integrin interactions and dynamics during cell migration by image correlation microscopy. *J Cell Sci* 117:5521–5534
- Wohland T, Shi X, Sankaran J, Stelzer EH (2010) Single Plane Illumination Fluorescence Correlation Spectroscopy (SPIM-FCS) probes inhomogeneous three-dimensional environments. *Opt Express* 18:10629
- Yamagata K, Yamazaki T, Miki H, Ogonuki N, Inoue K, Ogura A, Baba T (2007) Centromeric DNA hypomethylation as an epigenetic signature discriminates between germ and somatic cell lineages. *Dev Biol* 312:419–426
- Yguerabide J, Schmidt JA, Yguerabide EE (1982) Lateral mobility in membranes as detected by fluorescence recovery after photobleaching. *Biophys J* 40:69–75
- Zeskind BJ, Jordan CD, Timp W, Trapani L, Waller G, Horodincu V, Ehrlich DJ, Matsudaira P (2007) Nucleic acid and protein mass mapping by live-cell deep-ultraviolet microscopy. *Nat Meth* 4:567–569